Evaluation of thermally and chemically reduced graphene oxide films as counter electrodes on dye-sensitized solar cells

Manuel Rodríguez-Pérez [1,2], Julio Villanueva-Cab [1] and Umapada Pal [*1]

[1] *Instituto de Física, Benemérita Universidad Autónoma de Puebla,*
Apdo. Postal J-48, Puebla, Pue. 72570, México
[2] *Facultad de Ingeniería, Universidad Autónoma de Campeche, Campus V,*
s/n por Av. Ing. Humberto Lanz Cárdenas y Fracc. Ecológico Ambiental Siglo XXIII,
Colonia Ex Hacienda Kála. C.P.24085. San Francisco de Campeche, México

Abstract. Graphene oxide (GO) was prepared by modified Hummer's method to produce reduced graphene oxide (RGO) following standard thermal and chemical reduction processes. Prepared RGO colloids were utilized to fabricate RGO films over glass and FTO coated glass substrates through drop-coating. A systematic study was performed to evaluate the effect of reduction degree on the optical and electrical properties of the RGO film. We demonstrate that both the reduction process (thermal and chemical) produce RGO films of similar optical and electrical behaviors. However, the RGO films fabricated using chemically reduced GO colloid render better performance in dye sensitized solar cells (DSSCs), when they are used as counter electrodes (CEs). It has been demonstrated that RGO films of optimum thicknesses fabricated using RGO colloids prepared using lower concentration of hydrazine reducer have better catalytic performance in DSSCs due to a better catalytic interaction with redox couple. The better catalytic performance of the RGO films fabricated at optimal hydrazine concentration is associated to their higher available surface area and lower grain boundaries.

Keywords: graphene oxide; reduced graphene oxide; DSSC; graphe film

1. Introduction

Graphene, a two-dimensional crystalline form of carbon has shown its application potentials in several technological fields due to its favorable electrical, chemical and structural properties. Notwithstanding, despite such interesting properties, the use of graphene and graphene derivatives such as graphene oxide is limited by the impurities incorporated during their thermal and chemical processing. Although synthesis of highly pure graphene and graphene oxide is possible by chemical vapor deposition (CVD) process (Bae *et al.* 2010), the most common way to produce graphene derivatives like graphene oxide is through chemical oxidation of graphite to graphite oxide, and subsequent exfoliation (Becerril et al. 2008, Park and Ruoff 2009, Yin *et al.* 2010, Dreyer *et al.* 2011). Graphite oxide (GO) is typically synthesized either though Brodie (Brodie 1859, Boehm *et al.* 1967), Staudenmaier (1898), and Hummers (Hummers and Offeman 1958) methods, or any of their variants. In the cases of Brodie's and Staudenmaier's methods, a

---

∗Corresponding author, Professor, E-mail: upal@ifuap.buap.mx

combination of potassium chlorate ($KClO_3$), nitric acid (HNO_3) and/or sulfuric acid (H_2SO_4) is used to oxidize the graphite. In contrast, Hummer's method involves the treatment of graphite with potassium permanganate ($KMnO_4$) and sulfuric acid (H_2SO_4). It is well established that the most pure graphite oxide can be synthesized using Brodie's method, although it is the most time consuming method among the conventional ones (Boehm *et al*. 1967, Titelman *et al*. 2005). Nevertheless, in the cases of Staudenmaier or Hummers approach, there is a trade between time advantage and possible contaminations due to sulfur and excess permanganate ions (Park and Ruoff 2009). All the three synthesis routes result in the oxidation of graphite to various levels, containing aromatic and aliphatic groups such as hydroxyl, epoxy, ether, diol, ketones, etc. at their surface. Presence of these functional groups between GO sheets enhances their interlayer distances, facilitating their separation to individual GO sheets (exfoliation). Exfoliation of GO sheets is commonly achieved through the dispersion of GO powder in water, followed by sonication and/or mechanical stirring. The colloidal stability of the resulting dispersion strongly depends on its pH; while a pH 10 is seen to form stable colloids through electrostatic interactions (Li *et al*. 2008). Use of different organic solvents such as methanol, ethylene glycol, dimethyl formamide (DMF) has been seen to be effective for the dispersion of GO; even some of them has been used for the reduction of GO (Park *et al*. 2009, Yang *et al*. 2011). Reduction of graphene oxide is necessary for the elimination of the attached aromatic groups and consequent restoration of SP^2 groups in GO lattice. Presence of these groups generate different amount of lattice defects, affecting the electrical properties of GO.

Reduction of GO is commonly achieved using: (i) strong reductant such as hydrazine and its derivatives (Becerril *et al*. 2008, Li *et al*. 2008), metal hydrides such as sodium borohydrate (Shin *et al*. 2009), nitric acid, hydroiodic acid (Rath and Kundu 2015), ascorbic acid (Fernández-Merino *et al*. 2010) and other reducing agents (Paredes *et al*. 2008, Dreyer *et al*. 2011, Yang *et al*. 2011); (ii) through thermal reduction such as annealing at temperature above 800°C in inert atmosphere (Ar/H_2); (iii) rapid thermal annealing (> 2000°C/min) (Wang *et al*. 2008, Wu *et al*. 2009); (iv) low temperature (80-400°C) hydrothermal treatments (Zhou *et al*. 2009, Long *et al*. 2010); and (v) electrochemical reduction (Xu *et al*. 2013). Among all these processes, chemical reduction using hydrazine in combination with a thermal treatment at low temperature has shown to be a better process for obtaining highly conductive reduced graphene oxide films (Xu *et al*. 2011). However, the huge differences between the properties of the final products obtained using different synthesis and reduction processes, make it difficult to compare the GO and RGO obtained by different research groups.

The use of carbonaceous material such as graphene oxide (GO) and reduced graphene oxide (RGO) in dye sensitized solar cell (DSSC) has been carried out in different ways: (i) by incorporating graphene oxide sheets in semiconductor oxide matrix used as electrode; (ii) mixing redox coupled with GO or RGO to improve the electron mobility and reduction of liquid evaporation from the redox coupled solution; (iii) GO and RGO as counter electrodes (CE) replacing conventional Pt-based electrodes; and (iv) as a compact blocking layer made of a very thin GO layer (Roy-Mayhew and Aksay 2014). In all these cases, optimal concentration and/or thickness, and reduction degree of RGO are necessary, which again depend on the process used to obtain GO or RGO. To the best of our knowledge, there exists no literature report on a straightforward and systematic study to understand the effect of reduction process on the performance of RGO as counter electrode in dye sensitized solar cells.

In this work, we evaluated the optical and electrical properties of RGO obtained through thermal, chemical and a combination of both of these reduction processes. Subsequently the

fabricated RGOs were drop-coated over FTO glasses and utilized as counter electrodes (CEs) in dye sensitized solar cells. The effects of reduction steps or processes on the performance of DSSCs fabricated with RGO coated CEs were evaluated thought current-voltage and electrochemical impedance spectroscopy (EIS) measurements. Additionally, the concentration of hydrazine reductor and the thickness of RGO film were optimized for their application as CE in DSSCs. We demonstrate that the performance of RGO as CE in DSSC depends strongly on the availability of CE surface area rather than the degree of reduction of GO.

2. Methodology

2.1 Graphene oxide synthesis

Graphene oxide (GO) was prepared from graphite powder using a modified Hummers method (Park *et al*. 2010, Eigler *et al*. 2013). In brief, first, 5 g of graphite powder and 2.5 g of $NaNO_3$ were mixed in 230 mL of H_2SO_4 under mechanical stirring for 1 h, followed by 30 minutes ultrasonication. The resultant suspension was then kept inside an ice bath (10°C). After that, 30 g of $KMnO_4$ was added slowly under agitation, keeping the temperature of the suspension below 10°C. The resultant mixture was stirred continuously for 1 h inside the ice bath. Next, the ice bath was removed and the reaction mixture was heated to 35°C and kept at this temperature for 4 h. Then the heating was stopped and the mixture was left under agitation for 24 h. After that period, 460 mL of H_2O was added to the mixture slowly (1 h) and stirred for 30 minutes, which was followed by a heating at 98°C for 2 h. At the end of this heating period, 1400 mL of H_2O was added to the mixtures under stirring to bring its temperature down to room temperature. Then keeping the mixture in ice bath (10°C), 50 mL of H_2O_2 was added dropwise under agitation. The stirring process was continued for further 12 h keeping the mixture at room temperature. The product was separated from the mixture by centrifugation (4500 rpm, 15 min), washed with 15% of HCl solution and water (several times), and dried at ambient temperature.

2.2 GO films preparation

For films deposition, first the GO colloidal solution (0.25 mg/mL) was sonicated for 1 h in an ultrasonic bath (ElmaSonic P 60H). Then about 0.06 mL of GO colloidal solution was drop casted over a delimited area of 0.9×0.9 cm^2 of a glass slide (Madesa, USA) placed on a heating plate at 60°C. The process was repeated for several times to increase the thickness of the film. Finally the obtained films were annealed at 250°C for 1 h (2°C/min) in air to partially reduce the GO films (TRGO). The glass slides used as substrate were previously cleaned with liquid soap, NaOH solution of pH 9, and deionized water (18 Ω·cm) successively, and finally ultrasonicated for 15 min in isopropanol.

2.3 Reduction of GO

The chemically reduced graphene oxide was obtained following the procedure reported by Li and co-workers with some modifications (Li *et al*. 2008). About 5 mg of dry GO powder was dispersed in 20 mL of H_2O under magnetic stirring during 30 minutes, follow by a sonication with an ultrasonic T horn (30 Watts, 35% of Amplitude, Hielscher UP400S) for 30 min. Then about 70

μL of NH$_4$OH solution was added drop-wise to the mixture under magnetic stirring during 30 minutes. The final pH of the mixture was measured to be around 10.6. Next, a desirable amount (10, 20, 40, or 80 μL) of hydrazine monohydrate was added to the mixture, and stirred for 30 minutes in a sealed glass vial. The resultant colloidal solution was transfer to a Teflon lined (30 mL total volume) autoclave, sealed, and heated at 95°C (2°C/min) for 12 h. After cooling the autoclave to room temperature (25°C), the solution was taken out of the oven. The reduced graphene oxide prepared through the above process was designated as CTRGO. The same procedure used for fabricating GO films mentioned earlier (Section 2.2) was followed to fabricate the films using this CTRGO colloidal solution.

2.4 DSSC fabrication

2.4.1 TiO$_2$ paste for screen printing films

TiO$_2$ paste was prepared following a series of steps described previously in the literature (Ito *et al*. 2007). In brief, 0.5 g of Degusa-P25 was grinded on agate mortar, follow by the successive addition of 0.2 mL of acetic acid, 0.2 mL of H$_2$O, and 0.2 mL of anhydrous ethanol under continuous grinding. Each of the previous steps was repeated for 5 times. Then 0.4 mL of ethanol was added to the mixture and the grinding process was continued until it becomes dry. The latter step was repeated for another time. Obtained TiO$_2$ powder was then transferred from the mortar to a baker with an excess of ethanol (16 mL) and stirred with a magnetic bar during 1 minute, followed by sonication with a titanium ultrasonic T horn during 5 minutes. Then about 3.5 mL of terpineol was added drop-wise and the sonication steps described above were repeated. Then a previously prepared ethanolic solution of ethyl cellulose (0.05 g of ethyl cellulose in 5 mL of ethanol) was dropwise added to the TiO$_2$ mixture, stirrer and sonicated with the same procedure stated earlier. The resultant solution was stirred with a magnetic bar during 12 h; then the solution was heated at 75°C for 24 h to evaporate the ethanol. The solution was heated further at 110°C to evaporate the water, obtaining a viscus paste.

2.4.2 Fabrication and photovoltaic characterization of DSSC

Fluorine doped tin oxide (FTO, TEC 7, Aldrich) substrates were clean with soap, water, 2-propanol and acetone, with a sonication process of 15 minutes for each of the cleaning steps, followed by a heating process at 450°C during 1 h in air. TiO$_2$ films were deposited over FTO substrates by screen-printing using the TiO$_2$ paste prepared with Degusa-25. Five depositions were made for each FTO glass. After every deposition, the films were dried on a hot plate at 125°C. Finally, the films were sintered at 500°C for 2 h (5°C/min). The sintered films were heated at 120°C and soaked in a 10 mL dye solution (Z907 dye dissolved in tert-Butanol/acetonitrile (1:1 v/v)) during 20 hours for sensitizing. The films were washed with a mixture of tert-Butanol/acetonitrile (1:1 v/v) and dried to use in DSSC assembly. Platinum counter electrodes were prepared by drop-coating 2-propanol solution of H$_2$PtCl$_6$ (5 mM) over a delimited 0.9 × 0.9 cm^2 area over FTO glass, followed by heating at 450°C for 1 h. Both the photo anode (TiO$_2$ film over FTO glass) and the counter electrode were sealed in a sandwich configuration with Surlyn (60 μm). Finally, the electrolyte solution (0.6 M of 1-butyl-3-methylimidazolium iodide and 0.03 M iodine in acetonitrile/valeronitrile 85:15, v/v%) was introduced into the cell through a pair of holes previously perforated in the counter electrode which were subsequently sealed with Surlyn and thin glass pieces pressed under heat. Similar processes as described before were used to fabricate DSSCs with GO and RGO counter electrodes, but using GO or RGO CEs instead of the

platinum CE. Current density versus voltage J-V curves were obtained by illuminating the cells at 1 sun (100 mW/cm^2) and sweeping the applied bias from zero to the open circuit voltage V_{oc} with the help of a Keithley 4200-SCS galvanostat/potentiostat. Electrochemical Impedance Spectroscopy (EIS) was performed under dark, applying -0.45 V, scanning from 1 Hz to 1 MHz in a Zahner Zannium equipment.

2.5 Materials

Sulfuric acid (H$_2$SO$_4$, J.T. Baker 98%), hydrochloric acid (HCl, Meyer, 36.5-39%), acetic acid (J.T. Baker, 99.7%), ammonium hydroxide (Fermont, 28.7%), hydrogen peroxide (Merk, 30%), hydrazine monohydrate (Sigma-Aldrich, 98%), anhydrous ethanol (J.T. Baker, 94.7%), acetone (J.T. Baker, 99.7%), acetonitrile (Alfa Aesar, 99.7%), 2-propanol (J.T. Baker, 99.84%), tert-butanol (Sigma-Aldrich, $\geq$ 99.8%), anhydrous terpineol (Aldrich, 86480), valeronitrile (Aldrich, 99.5%), chloroplatinic acid solution (Aldrich, 8 wt% in H$_2$O), 1-Butyl-3 methylimidazolium iodide (Aldrich, $\geq$ 99%), ethyl cellulose (Sigma, 49-49.5% w/w), titanium (IV) oxide (Aldrich, 99.5%), iodine (Aldrich, 99.999%), sodium nitrate (NaNO$_3$, Sigma-Aldrich, $\geq$ 99%), potassium permanganate (KMnO$_4$, Sigma-Aldrich, $\geq$ 99%), sodium hydroxide (NaOH, J.T.Baker, 98.15%) were utilized as received, without further purification or processing. Deionized water (18 $\Omega\cdot$cm) from a Millipore system was utilized throughout the synthesis and processing.

2.6 Characterization technique

UV-vis absorption and/or transmission spectra were obtained using a Shimadzu UV-3101PC spectrophotometer. The spectra were taken from the reacted colloidal solution diluted by a factor of 10. Conductivity measurements on GO and RGO films prepared by drop-coating were carried out on a Jandel RM3000 test unit using a four-point-probe head with a pin-to-pin distance of about 1 mm. The thickness of the films was determined using a Veeco Dektak D-150 profilometer. Raman spectra of the GO and RGO samples were recorded in a termoelectrically cooled CCD attached Horiba LabRam-HR microRaman system under 632.8 nm He-Ne laser excitation. The morphology of the GO and RGO films were analyzed by a JEOL-JEM 211F transmission electron microscope, operating at 200 keV.

3. Results and discussion

The as-synthesized colloidal GO solution revealed a dark brown color (ocher), which after chemical (by solvothermal method) reduction (CTRGO) changed to dark. These colloidal solutions were stable, without precipitation even after 6 month of storage at ambient temperature. UV-Vis absorption spectra of the as-synthesized GO and CTRGO (reduced with different amounts of hydrazine) colloidal solutions are presented in Fig. 1. As can be observed, the signal related to π to $\pi*$ transition of the aromatic C = C bonds in the GO colloidal solution has a maximum absorbance at 229 nm (Zhou *et al.* 2009, Long *et al.* 2010). On chemical reduction with hydrazine under solvothermal process, this signal suffered a red shift, with peak appearing at 264 nm; suggesting the restoration of sp^2 carbon networks (Geng *et al.* 2010). An increase in hydrazine concentration during solvothermal treatment caused a reduction in the intensity of the signal, which can be related to the self-aggregation of graphene sheets into agglomerated particles (see Fig. 2).
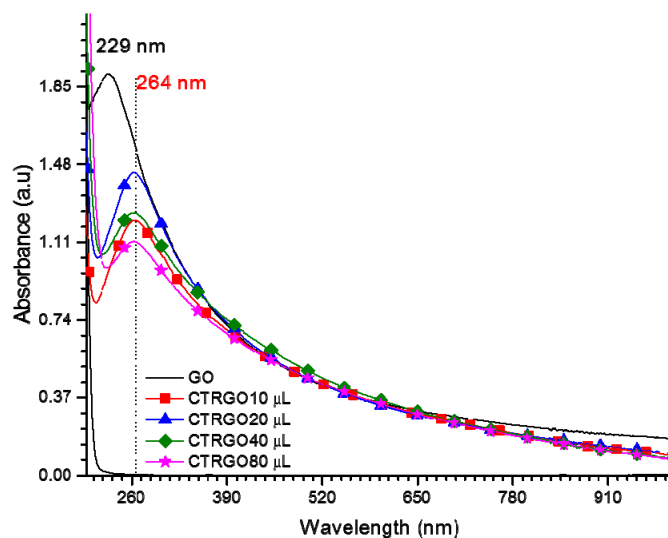
Fig. 1 UV-Vis absorption spectra of GO colloidal solution before and after chemical reduction with different amounts of hydrazine
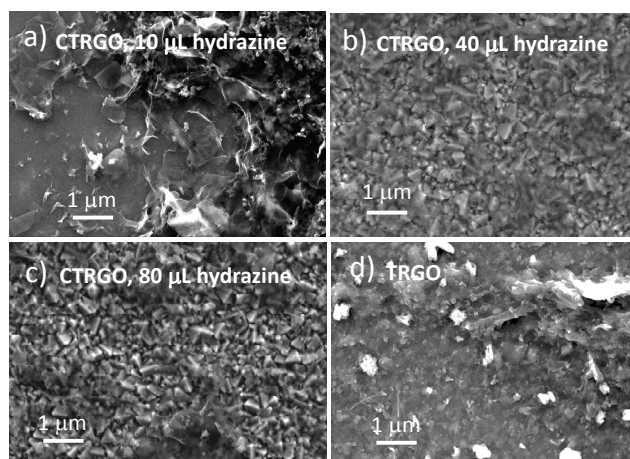
Fig. 2 Typical SEM images of the chemically and thermally treated GO films: (a) hydrothermally treated with 10 L of hydrazine; (b) hydrothermally treated with 40 L of hydrazine; (c) hydrothermally treated with 80 L of hydrazine; and (d) thermally treated at 250 °C for 1 h

Typical morphology of the chemically and thermally reduced GO films are presented in Fig. 2. As can be observed from Fig. 2(a), along with typical laminar structures of GO, there formed smaller compact particulate structures in the CTRGO films prepared with 10 L of hydrazine. On increasing the amount of hydrazine during hydrothermal treatment, almost all the laminar GO structures aggregated to form particle like structures. It is also clear from Figs. 2(b) and (c) that with the increase of hydrazine concentration, the size of the RGO grains reduces. On the other hand, the morphology of the TRGO film is completely different from the morphology of CTRGO films (Fig. 2(d)). Apparently, the thermal treatment caused a complete breackdown of the laminar

structure of GO to form aggregates of smaller sizes.

The Raman spectra of GO, TRGO and CTRGO deposited films are presented in Fig. 3. There appeared two characteristic Raman signals for GO, one at 1332 cm^{-1} (D band), associated to the breathing mode of A$_{1g}$ symmetry, and the other at 1595 cm^{-1} (G band), associated to the stretching motion of C Sp^2 atoms or E$_{2g}$ mode (Zhou *et al*. 2009, Qiu *et al*. 2014). The position of the G band shifted to 1589 cm^{-1} on reducing GO by hydrazine. Such a lower frequency shift of G band in GO has been associated to the bonding of impurity atoms and molecules at the surface of GO (Casiraghi *et al*. 2007, Gierz *et al*. 2008). To estimate the degree of reduction and defect concentration in RGO samples, we estimated the I_D/I_G ratio from the area under each of the component signals of the Raman spectrum. Generally, an increase in I_D/I_G ratio is the indication of enhanced reduction and increase of defect concentration at the GO surface. However, these defects can provide more active sites for the electrolyte reduction in DSSCs, and improve the catalytic activity of RGO counter electrode (Qiu *et al*. 2014). From the I_D/I_G ratio data presented in Fig. 2, we can see that both the thermal and chemical treatment enhances the I_D/I_G ratio in comparison with the ratio for GO film, without reduction treatment. It is interesting to note that both the thermal and chemical reduction process showed the same I_D/I_G ratio; indicating that it is possible to reduce GO by physical process such as thermal treatment, without using any reducing agent such as hydrazine.

As the initial evaluation of the counter electrodes fabricated using RGO films prepared by thermal and chemical reduction processes, the sheet resistance of the GO, TRGO and CTRGO films deposited over glass were measured by four-point probe technique. The measurements were performed over at least 6 sets of films (of same or different thicknesses) for each sample. The estimated sheet resistance and thickness of the samples are summarized in Table 1. As expected, the GO films without thermal or chemical treatment revealed highest sheet resistance of 234.8 MΩ/□. After thermal treatment at 250°C for 1 h, the sheet resistance of the film reduced by tree orders of magnitude (474.8 KΩ/□). A second layer of GO film was deposited over the previous one to analyze the sheet resistance of different samples (GO, TGO, CTRGO) with similar thicknesses. As shown in the Table 1, after the deposition of second GO layer and subsequent thermal treatment at 250°C for 1 h, the sheet resistance of the film reduced to 51.9 KΩ/□. The
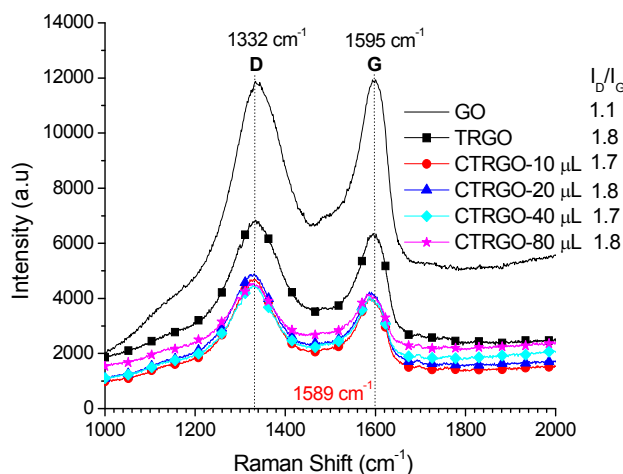
Fig. 3 Raman spectra of GO, TRGO and CTRGO films deposited over glass slide

sheet resistance of the RGO films made of solvothermally treated hydrazine reduced colloids varied considerably with the concentration of hydrazine. The RGO film prepared using lowest (10 μL) hydrazine concentration (i.e., sample CTRGO10 μL) revealed a sheet resistance 39.5 KΩ/$\square$, which is much lower than the sheet resistance of the TRGO film of similar thickness. However, the sheet resistance of the CTRGO films increases with the increase of hydrazine concentration. For example, the sheet resistance of the CTRGO film prepared using 80 μL of hydrazine was about 571.8 KΩ/$\square$. Similar variations of sheet resistance for the RGO films prepared by hydrazine reduction have also been observed by several other groups involved in monitoring in the conductivity on this material (Li *et al.* 2008, Xu *et al.* 2011). The increase of sheet resistance on increasing hydrazine concentration has been associated to the agglomeration of graphene oxide sheets at high hydrazine concentration of the colloidal solution during solvothermal process (Stankovich *et al.* 2007, Long *et al.* 2010). The agglomeration at higher hydrazine concentration is also clear from the SEM micrographs presented in Fig. 2. Such agglomeration causes an increase of grain boundaries, and reduces its electron mobility. From the results presented in Table 1, we can see that the sheet resistance of our thermally reduced GO film is very close to the sheet resistance of CTRGO films obtained with 10 μL of hydrazine, which is the lowest obtained sheet resistance among all the reduced GO films obtained in this work. The result indicates that a thermal treatment at 250°C in air for 1 h is good enough to reduce the GO films.

DSSCs were fabricated with FTO counter electrodes coated with differently reduced GOs, such as GO-FTO, TRGO-FTO, and CTRGO-FTO with different hydrazine concentrations, to evaluate their catalytic performance in assembled devices. For comparison, we also fabricated DSSCs with bare FTO and Pt-FTO as reference CEs. The current density versus voltage (J-V) curves obtained for DSSCs fabricated with different CEs are presented in Fig. 4. As we can see, the bare FTO counter electrode has very low catalytic activity with the redox couple, generating low current density (J_{SC}) and low fill factor (FF). The use of GO-FTO as counter electrode generates an improved catalytic activity, relative to bare FTO as CE, manifested by a significant increase of the current density (from 2mA/cm^2 to almost 4 mA/cm^2). The use of TRGO-FTO and CTRGO-FTO (for 10 μL and 40 μL of hidrazine) counter electrodes (of similar thicknesses) revealed similar J_{SC} (8.5 mA/cm^2) and almost the same open circuit photovoltage V_{OC} (0.6 V); however, with different fill factors (FF) and efficiencies (η). The RGO films fabricated with CTRGO colloidal solution

Table 1 Sheet resistance and average thickness of the GO, TRGO and CTRGO films fabricated over glass substrates

Sample	Sheet resistance	Thickness	Sheet resistance/thickness *
	(KΩ/$\square$)	nm	(KΩ/nm)
GO (unannealed)	234857	83.04	2828.24
TRGO 1 layer	475.89	85.04	5.59
TRGO 2 layers	51.99	145.03	0.36
CTRGO10 μL	39.57	160.13	0.24
CTRGO20 μL	58.63	121.03	0.48
CTRGO40 μL	106.37	120.81	0.88
CTRGO80 μL	571.88	114.85	4.98

*The sheet resistance/film thickness ratio is considered proportional to the resistivity of each film
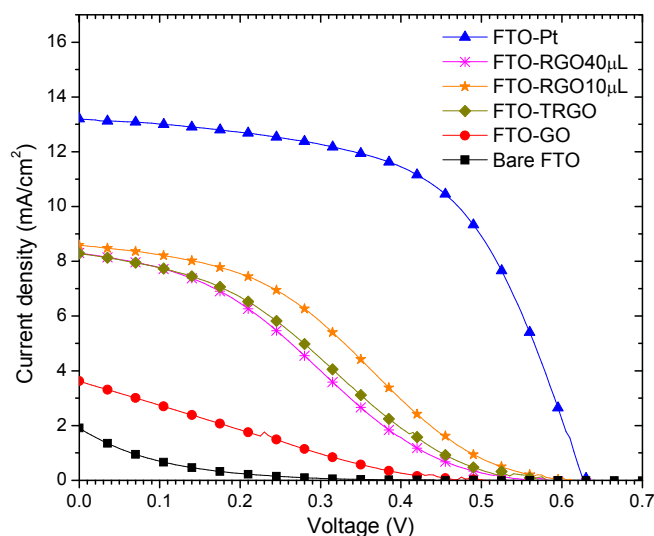
Fig. 4 J-V curves of the DSSCs fabricated with different counter electrodes

with 10 μL of hydrazine (CTRGO10 μL) showed best photovoltaic performance, with FF and η of 0.33 and 1.75, respectively.

From the J-V plots presented in Fig. 4, we can say that the use of RGO (FTO-CTRGO10 μL, FTO-CTRGO40 μL and FTO-TRGO) limits the electron injection to the oxidized redox couple, causing a slow catalytic activity, affecting directly the FF and η, compared with the platinized CE (FTO-Pt). Notwithstanding we observed an improvement in photocurrent using RGO. However, the results presented in Fig. 4 are not in agreement with the results obtained by Qiu *et al.* (2014), where a higher amount of hydrazine during GO reduction resulted in a better performance of DSSC, claiming a better catalytic activity for higher hydrazine concentration during chemical reduction. A summary on J_{SC}, V_{oc}, FF and η, for the best DSSCs fabricated are presented in Table 2.

Electrochemical impedance spectroscopy (EIS) measurements in dark, applying a reverse potential of -0.45 V in the frequency range 1 Hz to 1 MHz, were performed over DSSCs with different counter electrodes to analyze the total resistance (R_T) of the cells. In Fig. 5, we can observe that use of bare FTO as CE produces highest R_T, which is in good agreement with their

Table 2 Short circuit current density (J_{sc}), open circuit photovoltage (V_{oc}), fill factor (FF), and efficiency (η) of DSSC fabricated with different carbonaceous counter electrodes as catalytic material

Sample	Current density (mA/cm^2)	Voltage (V)	FF	η (%)
Bare FTO	1.91	0.44	0.082	0.07
FTO-GO	3.62	0.51	0.19	0.36
FTO-TRGO	8.28	0.58	0.29	1.42
FTO-TRGO10 μL	8.58	0.615	0.33	1.75
FTO-TRGO40 μL	8.3	0.58	0.27	1.34
FTO-Pt	13.19	0.63	0.56	4.75
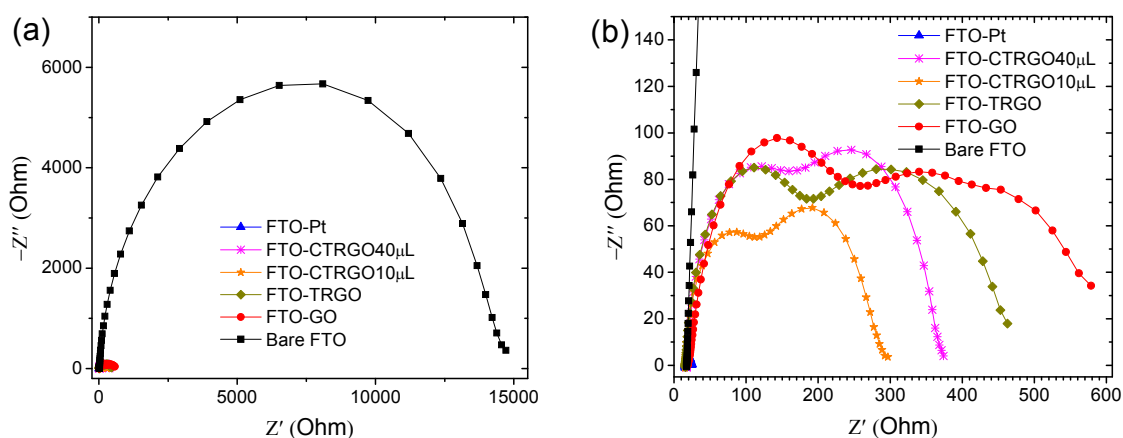
Fig. 5 Nyquist plot obtained for the DSSC's fabricated using different CEs, (a) from 0 to 14000 ohms (b) from 0 to 600 ohms. The measurements were performed in dark, applying a reverse potential of -0.45 V in the frequency range 1 Hz to 1 MHz

low photovoltaic performances presented in Fig. 4. The total resistance of the fabricated cells follows in descending order: FTO > GO-FTO > TRGO-FTO > CTRGO40 μL-FTO. The total resistance of the cell fabricated using counter electrode CTRGO10 μL-FTO was lowest among all the cells fabricated using GO or RGO in this work. However, their resistances were much higher than the cells fabricated using conventional Pt-FTO counter electrodes.

From Fig. 5, we can observe that the DSSC fabricated with TRGO-FTO as CE has a larger R_T than the DSSC fabricated with CTRGO10 μL-FTO. This result is in disagreement with the sheet resistance results obtained from four-probe data, where both the films (TRGO and CTRGO10 μL) revealed very similar sheet resistances for similar film thicknesses. This disagreement indicates that the sheet resistance is not the only parameter which controls the photocatalytic performance of RGO based CEs, as suggested by Qui *et al*. (2014). The improvement (reduction) of R_T is related to the defects or to the atoms/molecules such as N_2 bonded on the edge of RGO (Park *et al*. 2012), which enhance the interaction between RGO and I_3^-/I^- redox couple, improving the electronic injection on redox couple. As reported by Qui *et al*. (2014), we could expect a reduction of R_T with the increase of hydrazine concentration due to the presense of higher number of hydrazine atoms/molecules bonded on RGO surface. Notwithstanding in our case an increment on atoms and molecules bonded on the RGO surface to increase the amount of hydrazine produce an increment of R_T, which also cause a reduction of the surface area due to the GO agglomeration. Similar observations was made by Das and coworkers (Das *et al*. 2012), where an excessive doping of HNO_3 on graphene electrodes limits the active catalytic surface area of graphene. However, as the surface chemistries (attached ions, atoms, and molecules) of the RGO films prepared by hydrazine reduction and thermal reduction are very different, especially due to the incorporation of atomic nitrogen in hydrazine reduce RGO films (Park *et al*. 2012), it is very difficult to compare their electrocatalytic activities in DSSCs without a complete characterization of their surfaces.

As the DSSCs fabricated with CTRGO10 μL-FTO counter electrodes revealed better photovoltaic performance (and lowest R_T), the effects of film thickness on the sheet resistance and photovoltaics performance of the devices made of them were evaluated. For this study, films of different thicknesses were fabricated over glass/FTO substrates using 3, 5 and 10 consecutives

Table 3 Sheet resistance and film thickness of the CEs prepared with CTRGO10 μL

Sample	Number of layers	Sheet resistance (KΩ/$\square$)	Thickness nm
RGO10 μL	1	39.57 ± 19.92	160.13 ± 33.01
RGO10 μL	3	20.25 ± 6.51	289.99 ± 55.95
RGO10 μL	5	3.40 ± 0.79	393.98 ± 81.68
RGO10 μL	10	8.72 ± 1.99	625.62 ± 54.45
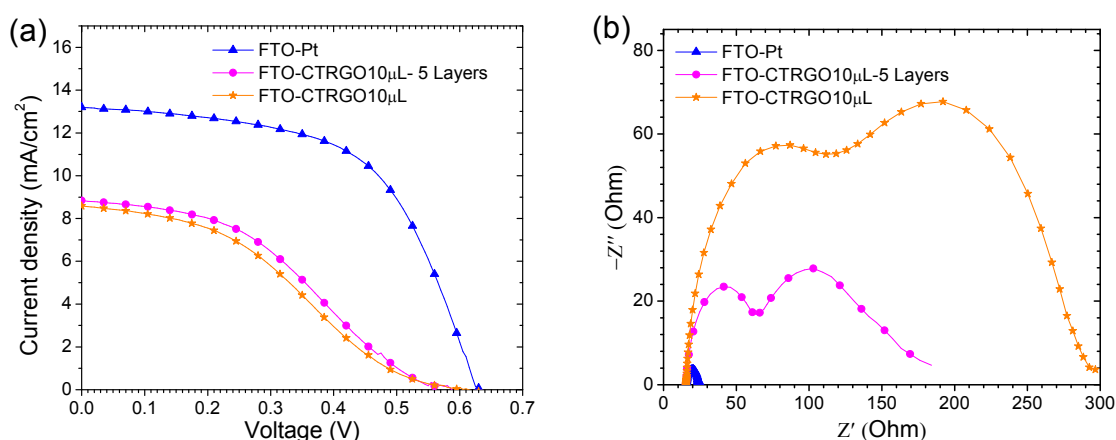
Fig. 6 (a) J-V curves; and (b) Nyquist plots for the DSSCs fabricated with CEs containing different thickness of CTRGO10 μL films

depositions of CTRGO10 μL colloidal solution, performing a drying step in between two successive depositions. The process was followed by a thermal process at 250°C in air for 1 h, as have been followed throughout this work. From Table 3, we can observe that an increase in film thickness causes a reduction in sheet resistance, producing a lowest sheet resistance of 3.4 kΩ/ for 400 nm (5 depositions) film. A further increase of film thickness (625 nm) causes an increase of sheet resistance. This optimum RGO film thickness (400 nm) is pretty close to the one published in the literature (Bae *et al.* 2010).

Finally, two new sets of DSSCs were fabricated using counter electrodes made of CTRGO10 μL-FTO with two different thicknesses of CTRGO10 μL layers to analyze their J-V and EIS characteristics (Fig. 6). As can be observed in Fig. 6(a), the J_{SC} of the cell fabricated with higher RGO layer thickness is a bit higher than the cell fabricated with thinner GRO layer (8.6 mA/cm^2 to 8.8 mA/cm^2), although the V_{OC} of both the cells remained same. At the result, the FF and hence the η for the former cell is a bit superior. Use of thicker RGO film at the CE produces a reduction of R_T by two folds, compared with the CEs with single RGO layer (orange curves and stars shaped data points in Fig. 6); which is related to an increase in the surface area of RGO due to the presence of higher amount of material, generating an increment on the catalytic activity of the CE with used redox couple.

4. Conclusions

In summary, we fabricated uniform GO and RGO films by drop-casting over FTO glass substrates for testing as counter electrode in DSSCs. Effects of thermal and hydrothermally treated hydrazine reduction processes on the sheet resistance and optical properties of the fabricated films have been studied. It has been observed that both the thermal and chemical reduction processes produce similar effects on the optical and electrical properties of RGO films. While a chemical reduction of GO at low hydrazine concentration produces well dispersed highly reduced RGO colloids which can be utilize to fabricate RGO coated FTO films of low sheet resistance, utilization of hydrazine reductor in high concentration induces aggregation of GO sheets. While both thermally and chemically reduced RGO can produce RGO films of similar/comparable sheet resistances, RGO films fabricated using optimal chemical reduction process have better catalytic activity for I_3^- reduction when utilized as counter electrode in DSSCs due to their higher contact surface area with the redox couple, and hence improved catalytic activity. It has been observed that the sheet resistance of RGO films fabricated using chemically reduced GO is not directly related to the extent of reduction; rather it depends on RGO surface area and grain boundaries in the multigrained films. The results presented in this study might be helpful for the designing graphene based counter electrodes for photovoltaic applications.

Acknowledgments

References

Bae, S., Kim, H., Lee, Y., Xu, X., Park, J.-S., Zheng, Y., Balakrishnan, J., Lei, T., Kim, H.R., Song, Y.I., Kim, Y.-J., Kim, K.S., Özyilmaz, B., Ahn, J.-H., Hong, B.H. and Iijima, S. (2010), "Roll-to-roll production of 30-inch graphene films for transparent electrodes", *Nat. Nano*, **5**(8), 574-578.

Bae, S., Kim, H., Lee, Y., Xu, X., Park, J.S., Zheng, Y., Balakrishnan, J., Lei, T., Kim, H.R., Song, Y.I. and Kim, Y.J.

Becerril, H.A., Mao, J., Liu, Z., Stoltenberg, R.M., Bao, Z. and Chen, Y. (2008), "Evaluation of solution-processed reduced graphene oxide films as transparent conductors", *ACS Nano*, **2**(3), 463-470.

Boehm, H.P., Eckel, M. and Scholz, W. (1967), "Untersuchungen am Graphitoxid V. Über den Bildungsmechanismus des Graphitoxids", *Zeitschrift für anorganische und allgemeine Chemie*, **353**(5-6), 236-242.

Brodie, B.C. (1859), "On the atomic weight of graphite", *Philos. Transact. Royal Soc. London*, **149**, 249-259.

Casiraghi, C., Pisana, S., Novoselov, K.S., Geim, A.K. and Ferrari, A.C. (2007), "Raman fingerprint of charged impurities in graphene", *Appl. Phys. Lett.*, **91**(23), 233108.

Das, S., Sudhagar, P., Ito, E., Lee, D.-y., Nagarajan, S., Lee, S.Y., Kang, Y.S. and Choi, W. (2012), "Effect of HNO_3 functionalization on large scale graphene for enhanced tri-iodide reduction in dye-sensitized solar cells", *J. Mater. Chem.*, **22**(38), 20490-20497.

Dreyer, D.R., Murali, S., Zhu, Y., Ruoff, R.S. and Bielawski, C.W. (2011), "Reduction of graphite oxide using alcohols", *J. Mater. Chem.*, **21**(10), 3443-3447.

Eigler, S., Enzelberger-Heim, M., Grimm, S., Hofmann, P., Kroener, W., Geworski, A., Dotzer, C., Röckert,

M., Xiao, J., Papp, C., Lytken, O., Steinrück, H.-P., Müller, P. and Hirsch, A. (2013), "Wet chemical synthesis of graphene", *Adv. Mater.*, **25**(26), 3583-3587.

Fernández-Merino, M.J., Guardia, L., Paredes, J.I., Villar-Rodil, S., Solís-Fernández, P., Martínez-Alonso, A. and Tascón, J.M.D. (2010), "Vitamin C is an ideal substitute for hydrazine in the reduction of graphene oxide suspensions", *J. Phys. Chem. C*, **114**(14), 6426-6432.

Geng, J., Liu, L., Yang, S.B., Youn, S.-C., Kim, D.W., Lee, J.-S., Choi, J.-K. and Jung, H.-T. (2010), "A simple approach for preparing transparent conductive graphene films using the controlled chemical reduction of exfoliated graphene oxide in an aqueous suspension", *J. Phys. Chem. C*, **114**(34), 14433-14440.

Gierz, I., Riedl, C., Starke, U., Ast, C.R. and Kern, K. (2008), "Atomic hole doping of graphene", *Nano Lett.*, **8**(12), 4603-4607.

Hummers, W.S. and Offeman, R.E. (1958), "Preparation of graphitic oxide", *J. Am. Chem. Soc.*, **80**(6), 1339-1339.

Ito, S., Chen, P., Comte, P., Nazeeruddin, M.K., Liska, P., Pechy, P. and Gratzel, M. (2007), "Fabrication of screen-printing pastes from TiO2 powders for dye-sensitised solar cells", *Prog. Photovoltaics*, **15**(7), 603-612.

Li, D., Muller, M.B., Gilje, S., Kaner, R.B. and Wallace, G.G. (2008), "Processable aqueous dispersions of graphene nanosheets", *Nature Nanotech.*, **3**(2), 101-105.

Long, D.H., Li, W., Ling, L.C., Miyawaki, J., Mochida, I. and Yoon, S.H. (2010), "Preparation of nitrogen-doped graphene sheets by a combined chemical and hydrothermal reduction of graphene oxide", *Langmuir*, **26**(20), 16096-16102.

Paredes, J.I., Villar-Rodil, S., Martínez-Alonso, A. and Tascón, J.M.D. (2008), "Graphene oxide dispersions in organic solvents", *Langmuir*, **24**(19), 10560-10564.

Park, S. and Ruoff, R.S. (2009), "Chemical methods for the production of graphenes", *Nat. Nano*, **4**(4), 217-224.

Park, S., An, J., Jung, I., Piner, R.D., An, S.J., Li, X., Velamakanni, A. and Ruoff, R.S. (2009), "Colloidal suspensions of highly reduced graphene oxide in a wide variety of organic solvents", *Nano Lett.*, **9**(4), 1593-1597.

Park, H., Rowehl, J.A., Kim, K.K., Bulovic, V. and Kong, J. (2010), "Doped graphene electrodes for organic solar cells", *Nanotechnology*, **21**(50), 505204.

Park, S., Hu, Y., Hwang, J.O., Lee, E.-S., Casabianca, L.B., Cai, W., Potts, J.R., Ha, H.-W., Chen, S., Oh, J., Kim, S.O., Kim, Y.-H., Ishii, Y. and Ruoff, R.S. (2012), "Chemical structures of hydrazine-treated graphene oxide and generation of aromatic nitrogen doping", *Nature Commun.*, **3**, 638.

Qiu, L., Zhang, H., Wang, W., Chen, Y. and Wang, R. (2014), "Effects of hydrazine hydrate treatment on the performance of reduced graphene oxide film as counter electrode in dye-sensitized solar cells", *Appl. Surf. Sci.*, **319**, 339-343.

Rath, T. and Kundu, P.P. (2015), "Reduced graphene oxide paper based nanocomposite materials for flexible supercapacitors", *Rsc Advances*, **5**(34), 26666-26674.

Roy-Mayhew, J.D. and Aksay, I.A. (2014), "Graphene materials and their use in dye-sensitized solar cells", *Chemical Reviews*, **114**(12), 6323-6348.

Shin, H.-J., Kim, K.K., Benayad, A., Yoon, S.-M., Park, H.K., Jung, I.-S., Jin, M.H., Jeong, H.-K., Kim, J.M., Choi, J.-Y. and Lee, Y.H. (2009), "Efficient reduction of graphite oxide by sodium borohydride and its effect on electrical conductance", *Adv. Function. Mater.*, **19**(12), 1987-1992.

Stankovich, S., Dikin, D.A., Piner, R.D., Kohlhaas, K.A., Kleinhammes, A., Jia, Y., Wu, Y., Nguyen, S.T. and Ruoff, R.S. (2007), "Synthesis of graphene-based nanosheets via chemical reduction of exfoliated graphite oxide", *Carbon*, **45**(7), 1558-1565.

Staudenmaier, L. (1898), "Verfahren zur Darstellung der Graphitsäure", *Berichte der deutschen chemischen Gesellschaft*, **31**(2), 1481-1487.

Titelman, G.I., Gelman, V., Bron, S., Khalfin, R.L., Cohen, Y. and Bianco-Peled, H. (2005), "Characteristics and microstructure of aqueous colloidal dispersions of graphite oxide", *Carbon*, **43**(3), 641-649.

Wang, X., Zhi, L. and Müllen, K. (2008), "Transparent, conductive graphene electrodes for dye-sensitized

solar cells", *Nano Lett*., **8**(1), 323-327.

Wu, Z.-S., Ren, W., Gao, L., Liu, B., Jiang, C. and Cheng, H.-M. (2009), "Synthesis of high-quality graphene with a pre-determined number of layers", *Carbon*, **47**(2), 493-499.

Xu, Y.X., Sheng, K.X., Li, C. and Shi, G.Q. (2011), "Highly conductive chemically converted graphene prepared from mildly oxidized graphene oxide", *J. Mater. Chem*., **21**(20), 7376-7380.

Xu, X.B., Huang, D.K., Cao, K., Wang, M.K., Zakeeruddin, S.M. and Gratzel, M. (2013), "Electrochemically reduced graphene oxide multilayer films as efficient counter electrode for dye-sensitized solar cells", *Sci. Rep*., **3**.

Yang, Y.K., He, C.E., He, W.J., Yu, L.J., Peng, R.G., Xie, X.L., Wang, X.B. and Mai, Y.W. (2011), "Reduction of silver nanoparticles onto graphene oxide nanosheets with N,N-dimethylformamide and SERS activities of GO/Ag composites", *J. Nanopart. Res*., **13**(10), 5571-5581.

Yin, Z., Sun, S., Salim, T., Wu, S., Huang, X., He, Q., Lam, Y.M. and Zhang, H. (2010), "Organic photovoltaic devices using highly flexible reduced graphene oxide films as transparent electrodes", *ACS Nano*, **4**(9), 5263-5268.

Zhou, Y., Bao, Q., Tang, L.A.L., Zhong, Y. and Loh, K.P. (2009), "Hydrothermal dehydration for the "green" reduction of exfoliated graphene oxide to graphene and demonstration of tunable optical limiting properties", *Chem. Mater*., **21**(13), 2950-2956.